Cell, Vol. 111, 825–836, December 13, 2002, Copyright ©2002 by Cell Press

Structure of Internalin, a Major Invasion Protein of *Listeria monocytogenes,* in Complex with Its Human Receptor E-Cadherin

Wolf-Dieter Schubert,[1] Claus Urbanke,[3] Thilo Ziehm,[1] Viola Beier,[1] Matthias P. Machner,[1] Eugen Domann,[4] Jürgen Wehland,[2] Trinad Chakraborty,[4] and Dirk W. Heinz[1,5]

[1]Department of Structural Biology
[2]Department of Cell Biology
German Research Center for Biotechnology (GBF)
Mascheroder Weg 1
D-38124 Braunschweig
Germany
[3]Institute of Biophysical Chemistry
Hannover Medical School
Carl-Neuberg-Str. 1
D-30623 Hannover
Germany
[4]Institute for Medical Microbiology
University of Giessen
Frankfurter Straße 107
D-35385 Giessen
Germany

Summary

***Listeria monocytogenes*, a food-borne bacterial pathogen, enters mammalian cells by inducing its own phagocytosis. The listerial protein internalin (InlA) mediates bacterial adhesion and invasion of epithelial cells in the human intestine through specific interaction with its host cell receptor E-cadherin. We present the crystal structures of the functional domain of InlA alone and in a complex with the extracellular, N-terminal domain of human E-cadherin (hEC1). The leucine rich repeat (LRR) domain of InlA surrounds and specifically recognizes hEC1. Individual interactions were probed by mutagenesis and analytical ultracentrifugation. These include Pro16 of hEC1, a major determinant for human susceptibility to *L. monocytogenes* infection that is essential for intermolecular recognition. Our studies reveal the structural basis for host tropism of this bacterium and the molecular deception *L. monocytogenes* employs to exploit the E-cadherin system.**

Introduction

Facultative intracellular bacteria including the opportunistic pathogen *Listeria monocytogenes* invade host cells to gain access to a nutrient-rich, shielded environment while evading host cellular defense mechanisms (Galan, 2000). To enter and survive within the host cells, pathogenic bacteria frequently exploit intracellular signal transduction mechanisms (Pieters, 2001; Kahn et al., 2002) through specific interactions with surface receptors (Cossart and Lecuit, 1998). *Listeria monocytogenes*, a ubiquitous, food-borne pathogen, leads to a systemic infection with high mortality rates particularly in immunocompromised individuals. The bacterium breaches major mammalian host barriers, entering through the intestine, and crossing the placenta and blood-brain barrier. Manifestations of listeriosis include diarrhea, meningitis, and fetal death (Lorber, 1997; Schlech, 2000).

Two listerial surface proteins mediate host cell specific internalization, internalin (InlA) (Gaillard et al., 1991) and internalin B (InlB) (Gaillard et al., 1991; Lingnau et al., 1995; Dramsi et al., 1995). They belong to a large group of surface-exposed leucine-rich repeat (LRR) proteins identified in the *Listeria* genome (Glaser et al., 2001; Cabanes et al., 2002). Internalins share a modular architecture comprising an N-terminal cap domain, a LRR-domain of 22 amino acid repeats, an interrepeat region (IR) domain, and varying C-terminal repeats. Most listerial LRR-proteins harbor both an N-terminal signal peptide and a C-terminal LPxTG motif followed by a hydrophobic transmembrane region, marking them as extracellular proteins, processed by a sortase, and covalently attached to the bacterial cell wall peptidoglycan (Garandeau et al., 2002; Bierne et al., 2002). Crystal structures of the cap/LRR-domain of InlB (Marino et al., 1999) as well as the cap/LRR/IR-domain of InlB and InlH (Schubert et al., 2001) indicate a curved solenoid for the LRR-domain structurally related to other LRR-proteins (Kobe and Kajava, 2001).

InlA was the first molecule identified enabling *L. monocytogenes* to invade non-phagocytic cells such as those of the human intestinal epithelium (Gaillard et al., 1991). InlA is sufficient for adhesion to and inducing uptake into epithelial cells. Its eukaryotic target is the surface receptor E-cadherin (Mengaud et al., 1996; Lecuit et al., 1997). Extracellularly, E-cadherin ensures tight adhesion of neighboring epithelial cells through homotopic interactions in adherens junctions on their basolateral side (Uemura, 1998). Intracellularly, E-cadherin is linked to the actin cytoskeleton through intervening proteins and is critical for physiological processes such as cell signaling and differentiation, but also diseases like cancer (Steinberg and McNutt, 1999). E-cadherin consists of five extracellular, immunoglobulin-like domains (EC1 to EC5), a transmembrane α-helix, and an extended intracellular domain that binds β-catenin. Known structures of cadherin domains include extracellular murine E-cadherin (EC1, Overduin et al., 1995; EC1-EC2, Nagar et al., 1996; Pertz et al., 1999), murine N-cadherin (EC1, Shapiro et al., 1995; EC1-EC2, Tamura et al., 1998), C-cadherin (EC1-EC5, Boggon et al., 2002), and the cytoplasmic domain in complex with β-catenin (Huber and Weis, 2001). The extracellular, N-terminal domain of E-cadherin (EC1), responsible for the specificity of *trans*-interactions between identical cadherins on neighboring cells, was also found to be the target of InlA (Lecuit et al., 1999). The observation that InlA does not adhere to murine epithelia was traced to residue 16 of EC1. Replacement of Pro16 in human EC1 by glutamate in mice renders these resistant to InlA-triggered bacterial invasion (Lecuit et al., 1999). An animal model for the first step of human listeriosis was created by transgenically

[5]Correspondence: dih@gbf.de

expressing human E-cadherin in the mouse intestine (Lecuit et al., 2001).

To investigate the host tropism displayed by internalin at a structural level, we herewith describe the crystal structures of the functional domain of InlA (InlA′) both uncomplexed and in functional complex with the N-terminal domain of its human receptor E-cadherin (hEC1). This structural analysis provides a detailed picture of the first steps leading to human infection by *L. monocytogenes*, revealing important insights into fundamental events of bacterial pathogenesis.

Results

Structure of InlA′

InlA′, comprising the first 460 residues of mature InlA (residues 36–496), is an elongated, sickle-shaped molecule, 108 Å long and 27 Å in diameter (Figure 1). Structurally, InlA′ consists of three distinct domains characteristically fused into a contiguous domain, the "internalin domain" previously described for InlB and InlH (Schubert et al., 2001). Though InlB and InlH are significantly smaller, the constituent domains are structurally conserved and will be described only briefly.

Residues 36 to 78 (pink domain in Figure 1A) form a compact α-helical domain, encompassing three α helices and no significant β strands.

Residues 79 to 414 (violet domain) constitute an LRR-domain consisting of fifteen and a half 22 residue repeats. Together they create a right-handed solenoid, each repeat adding a helical turn. A conserved pattern of aliphatic hydrophobic residues and an asparagine directed toward the solenoid core characterizes each repeat (Marino et al., 1999; Schubert et al., 2001). Each LRR begins with a β strand of five residues (xxLxL, L: leucine, valine, or isoleucine, x: any amino acid) followed by a seven-residue loop (xxNxLxx), a five-residue 3_{10}-helix (LxxLx), and a second five-residue loop (xLxxL) (Figure 1A). The β strands combine to form a 16 stranded, parallel β sheet. The fifteen 3_{10}-helices, spatially larger than the β strands, introduce an overall curvature to the ensemble in which the β sheet and the 3_{10}-helices, respectively, define the inner, concave, and the outer, convex surfaces. Each repeat is additionally rotated by ∼5° around the solenoid axis relative to its predecessor adding a twist to the overall arrangement. Residues 415 to 495 (blue in Figure 1A) are best described as immunoglobulin (Ig)-like (Schubert et al., 2001), with a conserved a-g-f-c β sheet of the V-set of Ig-domains but a shortened d-e-b sheet (Leahy, 1997). This region is structurally the most flexible part of the internalin domain, small differences being obvious when comparing InlA′, InlB′ and InlH′ (Schubert et al., 2001) but also when comparing InlA′ in different crystal packing arrangements.

Structure of E-Cadherin

The domain hEC1, here bound to InlA′, is the first structure of a human E-cadherin. As expected, it is structurally very similar to other EC1 domains (Figure 3). hEC1 consists of seven β strands arranged in two antiparallel β sheets respectively comprising strands a′-b-e-d and c-f-g-a (Figures 1B and 1C) closely related to the immunoglobulin fold (Shapiro et al., 1995). The side chain of Trp2 fills a hydrophobic pocket within hEC1, as observed in one crystal packing of murine EC1 (Pertz et al., 1999). Most cadherin crystal structures instead show a strand-exchange between neighboring EC1 domains placing Trp2 into the corresponding pocket of the second molecule (Shapiro et al., 1995; Nagar et al., 1996; Tamura et al., 1998; Boggon et al., 2002). Unlike the structure of Pertz et al. (1999), however, the N-terminal half of β strand a (a′ in Figure 3) closely associates with strand b. The C-terminal half of strand a hydrogen bonds to strand g (as in other cadherins) resulting in an overall resemblance to V-type Ig-domains (Leahy, 1997). Presently, it is not clear whether the conformation of β strand a′ represents the relaxed monomeric form of hEC1 or whether this is induced through close contact with InlA′. In addition to residues 1 to 100 of hEC1, three N-terminal residues, introduced by the cloning methodology (Pro(-2), Leu(-1), and Gly0) are well ordered in the electron density and form part of the structure.

The InlA′/hEC1 Complex

InlA′ and hEC1 form a stoichiometric complex in which InlA′ binds the smaller hEC1 in a tight embrace, clearly reminiscent of the ribonuclease inhibitor binding its target ribonuclease A (Kobe and Deisenhofer, 1995). hEC1 in turn occupies and fills the central cavity created by the curved LRR-domain of InlA′. In contrast to the planar, horseshoe shape of the ribonuclease inhibitor, the LRR of InlA′ is additionally twisted out of a central plane creating a pseudo-helical surface for hEC1 binding (Figure 3). The cavity is created by the 16 stranded parallel β sheet of InlA′ (Figures 1 and 2). The major axis of hEC1 roughly aligns with the β strands of InlA′ such that the interconnecting loops of hEC1 lie above and below the twisted interaction plane. The C termini of hEC1 and InlA′, furthermore, point in opposite directions (Figure 2). In vivo both domains are followed by spacer domains that link the molecules to opposing cell surfaces. The relative orientation of hEC1 thus allows an optimal approach of the bacterial protein poised to recognize and bind its counterpart hEC1.

The extended interface between InlA′ and hEC1 stretches over the entire inner, concave surface of InlA′. Conversely, InlA′ covers more than 180° of the circumference of hEC1 (Figure 2C). In InlA′, the interface exclusively involves the LRR-domain (Figure 4A). Though near, both adjacent domains of InlA′ do not contact hEC1. Their function thus is presumably structural: capping the hydrophobic core.

The InlA′/hEC1 Interface

InlA′ and hEC1 respectively contribute 1160 Å^2 and 1240 Å^2 to the accessible surface area of interaction. The total area of 2400 Å^2 is larger that the "standard" interface area observed for other noncovalent protein complexes (1600 ± 400 Å^2; Lo Conte et al., 1999) though not exceptionally large. Amino acids involved in contacts to hEC1 are exclusively β strand residues or immediately adjacent (Figures 1D and 4A). Most repeats provide one or two residues for binding hEC1. Exceptions include LRR12 and 13, each of which provides four such residues, while LRR3 and 10 do not participate in bind-

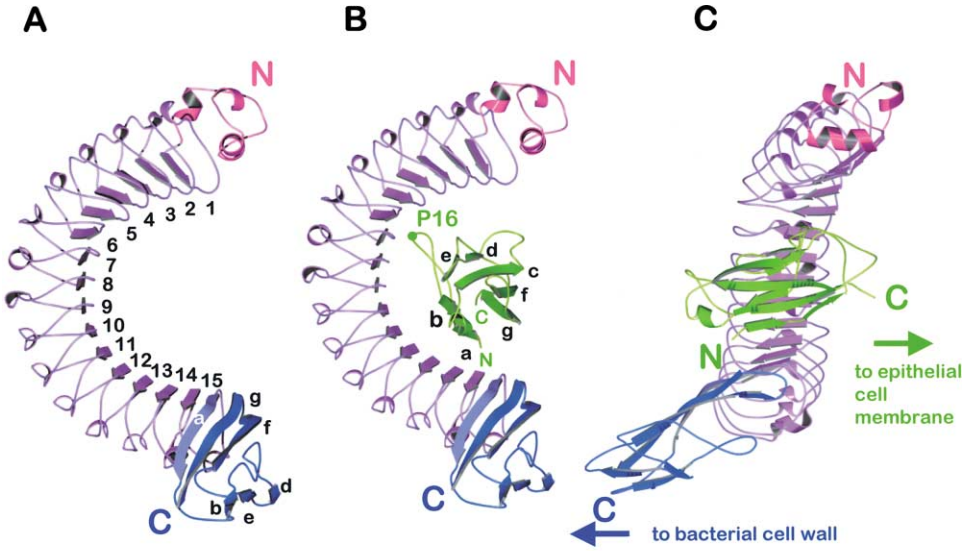

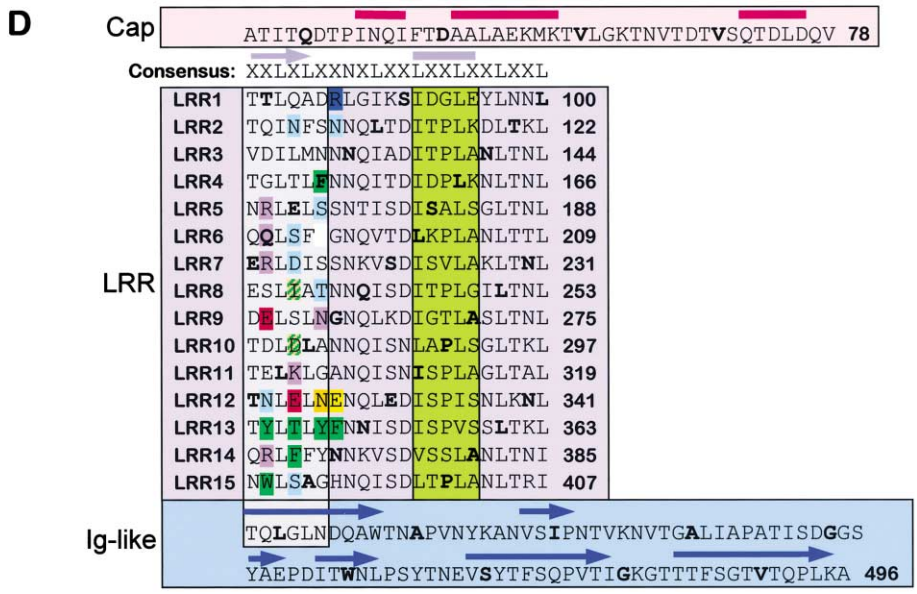

Figure 1. Structure of InlA′

(A) Uncomplexed InlA′: cap domain-pink, LRR-domain-violet, Ig-like interrepeat domain-blue. β strands of the LRR are numbered; those of the Ig-like domain are indicated by letters.

(B) The complex InlA′/hEC1 viewed as in (A) and (C) rotated by 90°: hEC1 is rendered in green, strands indicated by letters.

(D) Primary and secondary structure of InlA′: Every tenth residue in bold. The three domains are shown as rectangles color-coded as in (A). Secondary structure is indicated by bars (α-/3_{10}-helices) and arrows (β strands). The LRRs are aligned and labeled; the conserved β sheet and 3_{10}-helices are highlighted by gray and green boxes. Individual residues involved in intermolecular contacts are underlaid by colored boxes: Blue/red – positively/negatively charged partners of salt bridges; violet – hydrogen bond; green/striped green – hydrophobic/unfavorable interactions; cyan – hydrogen bond to bridging water molecule, orange/yellow – ligands to Cl^-/Ca^{2+}.

ing. The region defined by LRR12 to 15 is most extensively involved in interactions. It contains a patch of aromatic amino acids engaging in hydrophobic contacts to Val3 and Ile4 of hEC1 and provides the ligands to both the bridging Ca^{2+} and Cl^- (see below).

A deletion of one amino acid in β strand 6 (shortening LRR6 to 21 residues, Figure 1D) creates a hydrophobic pocket between itself and the neighboring repeats 5 and 7 (Figure 4B). This hydrophobic pocket accommodates Pro16 of hEC1, a residue crucial for recognition of human E-cadherin by InlA (Lecuit et al., 1999, 2001). Strikingly this is the only interaction between InlA′ and hEC1 involving main-chain atoms from InlA′. Murine E-cadherin in which Pro16 from hEC1 is replaced by glutamic acid is not recognized by InlA (Lecuit et al., 1999). Replacing Pro16 by glutamic acid in silico (Figure 4B) indicates that glutamate both sterically and by its hydrophilic/charged nature prevents a close approach of both

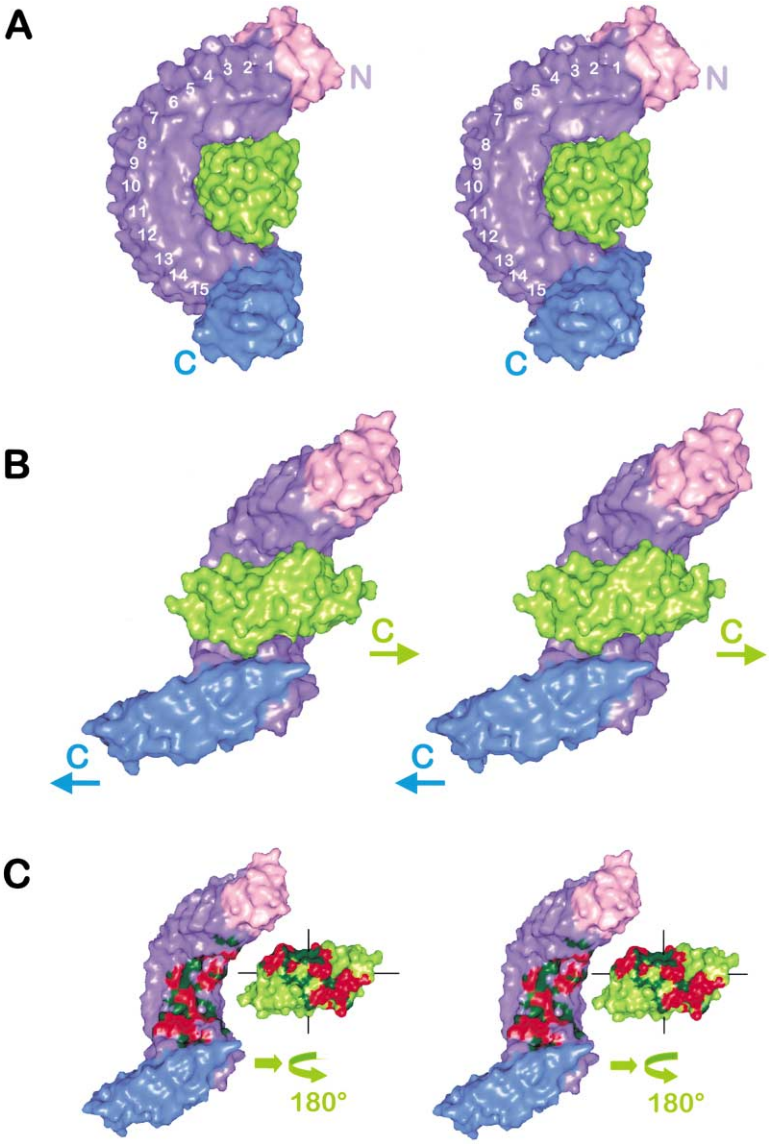

Figure 2. Stereographical Representation of the Molecular Surface of the Complex InlA′/hEC1

(A) View onto the interaction plane and (B) rotated by 90° around the vertical axis.
(C) A representation of the interaction surface between the two proteins. The molecular surfaces contributed by residues involved in protein-protein-interactions are rendered in red, those involved in contacts to bridging water molecules in dark green. To open up the complex, hEC1 has been shifted along its major axis and rotated by 180° around the vertical axis as indicated.

proteins. The pivotal role of Pro16 as a specific determinant for complex formation is thus confirmed.

The parts of hEC1 in closest contact with InlA′ are β strands a, b, and the intermediate loop ab (Figures 1B and 4A). Residues within this region with an individual share of more than 3% of the interface surface area include Val3, Ile4, Pro5, Pro6 (β strand a), Lys14, Pro16, Phe17, Pro18, Lys19 (loop ab), Gln23, Lys25, and Asn27 (β strand b). The loop Pro16-Lys19 forms a conspicuous protrusion in which both Pro16 and Pro18 adopt a *cis*-conformation and Pro18 stacks upon Phe150 of InlA′. C-terminal residues with a similar contribution to the interface surface include only Val48 (loop cd), Trp59 (strand e), Glu64 (loop ef), and Met92 (strand g).

Ions at the Interface

The crystallization conditions used for the complex of InlA′ and hEC1 include 50 mM $CaCl_2$, as Ca^{2+} was found to influence the binding affinity between the two (see below). Correspondingly, two electron density peaks at the interface between InlA′ and hEC1 were respectively interpreted as Ca^{2+} and Cl^- (yellow and orange sphere in Figure 4A). The Ca^{2+} has an octahedral coordination sphere involving five water molecules and Glu326 of InlA′ (Figure 4C). The average coordination distance is 2.45 Å. While InlA′ is directly involved in coordinating Ca^{2+} through Glu326, interaction to Asp29 of hEC1 is mediated by two bridging water molecules. The irregular coordination sphere of Cl^- has an average coordinating distance of 3.30 Å to five neighboring groups: N^{γ}-Asn282 and N^{γ}-Asn325 of InlA′, N^{η}-Lys25 of hEC1 and two water molecules. Cl^- thus also bridges both proteins, though it forms a salt bridge only to hEC1.

A second Ca^{2+}-site not located at the interface is equivalent to one of the interdomain Ca^{2+}-sites observed for multi-domain cadherin structures (Nagar et al., 1996; Tamura et al., 1998; Boggon et al., 2002). Conformational changes to hEC1 induced by InlA′ thus do not extend beyond hEC1. Interestingly, InlA′ crystal form C2-I also binds Ca^{2+} within the interface region. This,

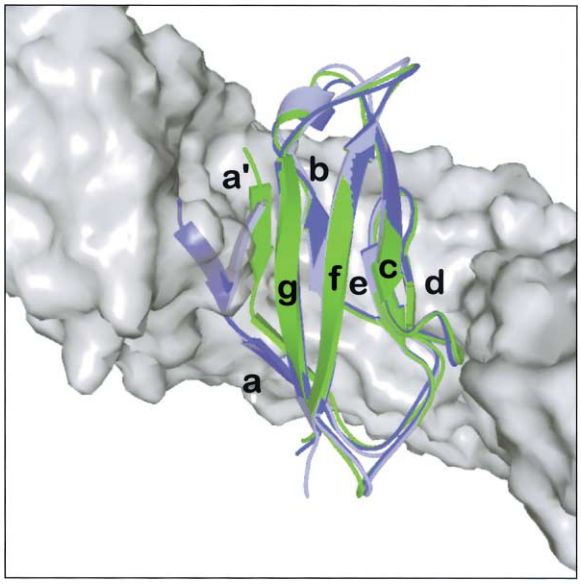

Figure 3. The N-Terminal Domain of E-Cadherin

Superposition with related murine domains: Green – hEC1 (this paper); light blue – murine E-cadherin (Pertz et al., 1999); blue – murine N-cadherin (Tamura et al., 1998). β strand a′ is more closely associated with strand b in hEC1 and is important for intermolecular contacts between hEC1 and InlA′.

however, does not involve the physiological coordination by Glu326.

Biophysical Characterization of InlA′/hEC1

InlA′ and hEC1 are both highly soluble proteins showing no precipitation either in water or high salt concentrations (1 M NaCl or $CaCl_2$). Affinity chromatography (see below) indicates a pH-optimum for InlA′/hEC1 complex formation of roughly 7.0 and saturated binding at 20 mM $CaCl_2$ (not shown). Ca^{2+} is thus required for optimal interaction between InlA′ and hEC1 (see above). Analytical ultracentrifugation indicates a sedimentation coefficient of 1.5 S for free hEC1 and 3.1 S for InlA′. Mixtures of hEC1 and InlA′ reveal two sedimenting boundaries at ~1.5 S (hEC1) and ≥3.1 S. The increase in the sedimentation coefficient of the second boundary correlates with the ratio of hEC1:InlA′ and is therefore assigned to complex formation (black line in Figure 5). Boundaries sedimenting with more than 3.1 S were only observed in mixtures of hEC1 and InlA′, never for individual proteins (with Ca^{2+} or without) excluding the possibility of Ca^{2+}-induced protein aggregation. The relative height of the sedimenting boundaries derived from an integrated Gaussian curve fitting (Machner et al., 2001) indicate the proportion of free and complexed hEC1 from which the affinity constant between the two proteins is estimated to be 50 ± 30 μm in Ca^{2+}-free buffer. This increases to 8 ± 4 μm in the presence of 20 mM $CaCl_2$. Binding of hEC1 by InlA′ is thus surprisingly weak, but enhanced by the addition of $CaCl_2$.

The observed affinity of InlA′ for hEC1 is stronger than the affinity constant of ~64 μM for dimer formation of the complete extracellular domain (EC1–EC5) of C-cadherin (Chappuis-Flament et al., 2002). Dimer formation for isolated EC1 is not observed, a finding that our analyses confirm.

Contribution of Individual Residues to Binding

Surface-exposed, aromatic amino acids of InlA′ dominate the direct interactions with hEC1. Phe150 is instrumental in positioning Pro18 of hEC1 (Figures 4A and 4B). Tyr343, Tyr347, Phe367, Tyr369, and Trp387 belong to a cluster of aromatic residues in LRR13 to 15 (Figure 4A) that interact with Val3, Ile4, Pro5, Pro6 in β strand a of hEC1, and a group of polar residues in β strand b (Gln23, Lys25, and Asn27). Replacing the aromatic residues individually by alanine and repeating the sedimentation experiments indicates that most mutations reduce affinity for hEC1 to an extent that precludes reliable quantification of the binding affinity (Figure 5A, F150A, Y343A, F367A, and W387A). The binding affinity of mutant Y347A for hEC1 is reduced but still quantifiable at a third to a half that of the wild-type protein. Mutant Y369A exhibits the opposite effect, revealing a slight, yet significant increase in binding affinity for hEC1 as compared to the wild-type protein. This confirms the observation that Tyr369, though partly disordered in the crystal structure, engages in an unfavorably close contact with Asn27 of hEC1. Removal of the bulky side chain presumably removes this strain improving overall binding affinity.

Similar experiments were performed with mutants of hEC1. Pro16 was replaced by alanine, valine, aspartate, and glutamate (Figure 5B) to analyze this interaction in more detail. All four mutants abolish binding to InlA′. Extended, charged residues like aspartate and glutamate clearly introduce a severe steric clash with the binding pocket of Pro16 (Figure 4B). Medium-sized (valine) to small (alanine) hydrophobic residues are, however, also incapable of replacing Pro16, presumably because they are unable to adopt the energetically unfavorable *cis*-conformation of Pro16. A proline in position 16 is thus strictly required for binding between hEC1 and InlA′.

Trp2 of hEC1 has recently been reinterpreted to be critical for *trans*- (rather than *cis*-) interactions between cadherins from neighboring cells through an inter-strand exchange (Boggon et al., 2002). To investigate its role in molecular stability in hEC1 and in complex formation, it was alternatively replaced by alanine, serine, and aspartate. InlA′ binds none of these mutants indicating that Trp2 is crucial for the N-terminal β strand to adopt its native conformation. The mutant W2D in absence of InlA′ reveals a distinct lowering of the sedimentation coefficient (1.5 to 1.0) indicating a partial unfolding of this hEC1 variant.

Discussion

LRR6 of InlA′ Functions as a Hinge

The structure of InlA′ is presented in three unrelated crystal environments: (1) an uncomplexed state with a free binding site (C2-I), (2) an uncomplexed state in which the binding site is occupied by a symmetry-related molecule (C2-II), and (3) in complex with hEC1. Comparing C2-I to C2-II indicates an overall widening of the molecular grip on filling of the central void. Super-

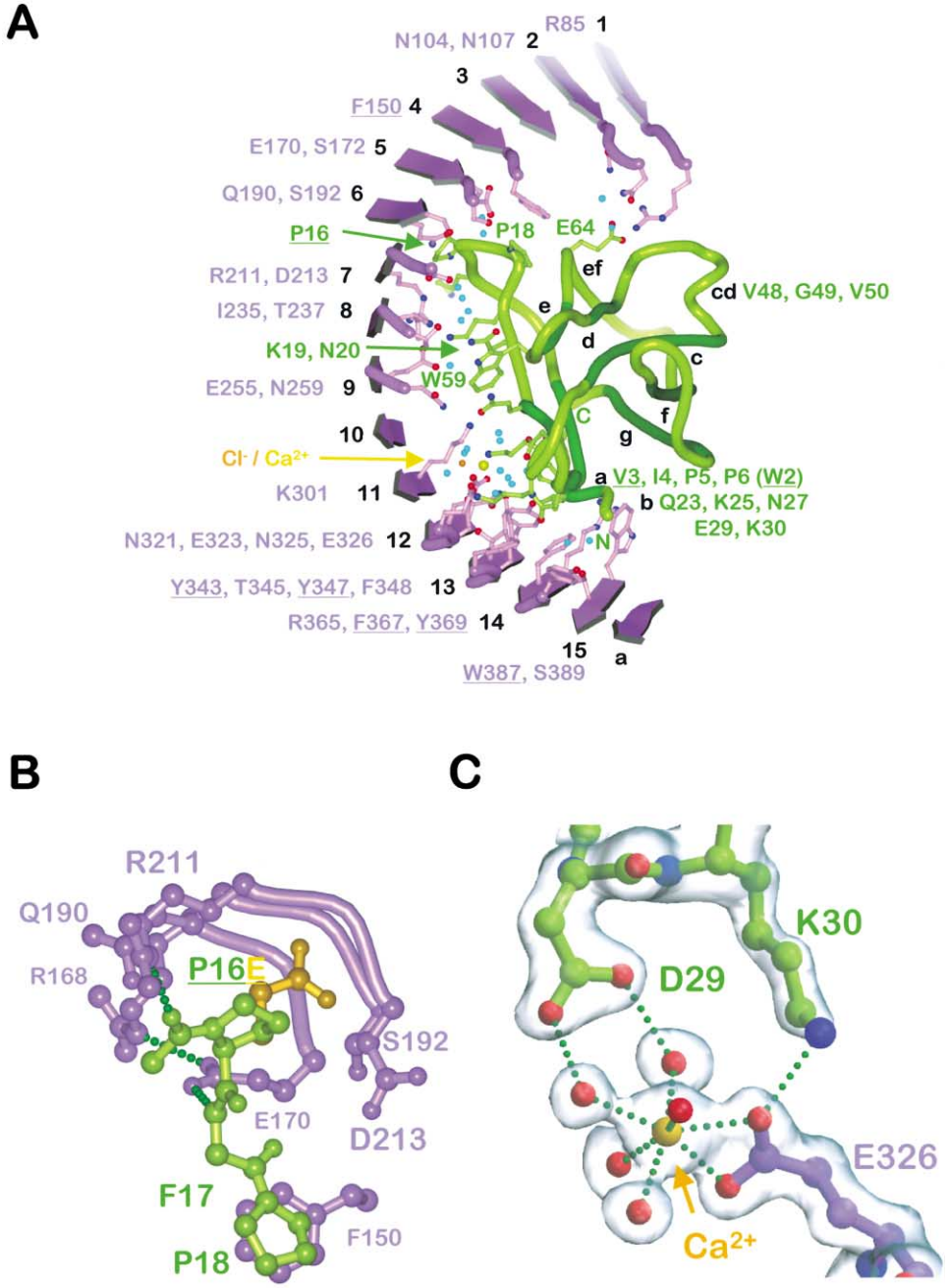

Figure 4. Detailed View of the Interactions between InlA′ and hEC1

(A) All residue side chains involved in direct interactions or as ligands to bridging ions/water are indicated in ball-and-stick representation. Residues mutated in this study are underlined. For InlA′ β strands (1–15 and a of Ig-like domain) and adjacent coils are shown in violet. hEC1 is represented by a continuous coil, β strands are indicated by dark-green shading (labels a–g, connecting loops are indicated by two letters to indicate flanking β strands). Cyan-, yellow- and orange-colored spheres represent water, Ca^{2+}, and Cl^{-}, respectively.

(B) View of the hydrophobic pocket in InlA′, which accommodates Pro16 of hEC1. In addition, the neighboring residues Phe17 (side chain omitted) and Pro18 are involved in specific interactions with InlA′. Hydrogen bonds are indicated by green dotted lines. In murine, E-cadherin Pro16 is replaced by glutamate (yellow model).

(C) The octahedrally coordinated Ca^{2+} bridging InlA′and hEC1. The refined $2F_O$-F_C map contoured at 1σ is shown as a translucent surface.

imposing the nine C-terminal LRRs of C2-I and C2-II reveals a virtually unchanged conformation. Instead LRR6, whose repeat length is shortened to 21 residues (see above), functions as a hinge causing the 5 N-terminal LRRs to tilt relative to the C-terminal repeats. Filling the binding site with its physiological binding partner hEC1 widens the hinge angle even further (Figure 6, violet structure as compared to uncomplexed, gray

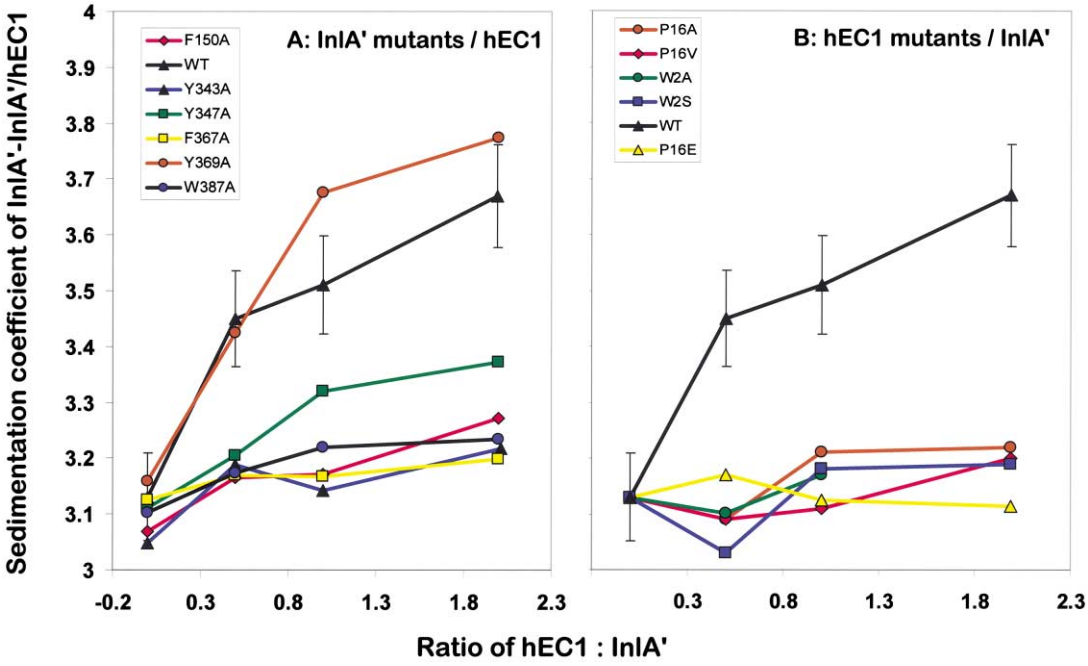

Figure 5. Detection of InlA′/hEC1 Interaction by Analytical Ultracentrifugation

InlA′ or its mutants (A) are titrated with indicated amounts of hEC1 or the respective mutants (B). An increase in the sedimentation coefficient of the faster moving boundary indicates complex formation. Sedimentation coefficients are determined with an error of ± 2.5% as indicated for the data on wild-type (WT) InlA′.

structure). LRRs are thus overall quite rigid. Where needed, flexibility is specifically introduced by upsetting a single LRR-motif.

Among the internalins of *L. monocytogenes*, InlA is unique in possessing a LRR of 21 amino acids. By contrast, YopM, a LRR protein from *Yersinia pestis*, has 12 repeats of 20 residues, while the remaining three contain 22 residues (Evdokimov et al., 2001). Nevertheless YopM superimposes particularly well on the nine C-terminal repeats of InlA′ (Figure 6) due to an identical twist in the β sheet. The difference of the 21-residue repeat of InlA′ to the 20-residue repeats of YopM is that the missing

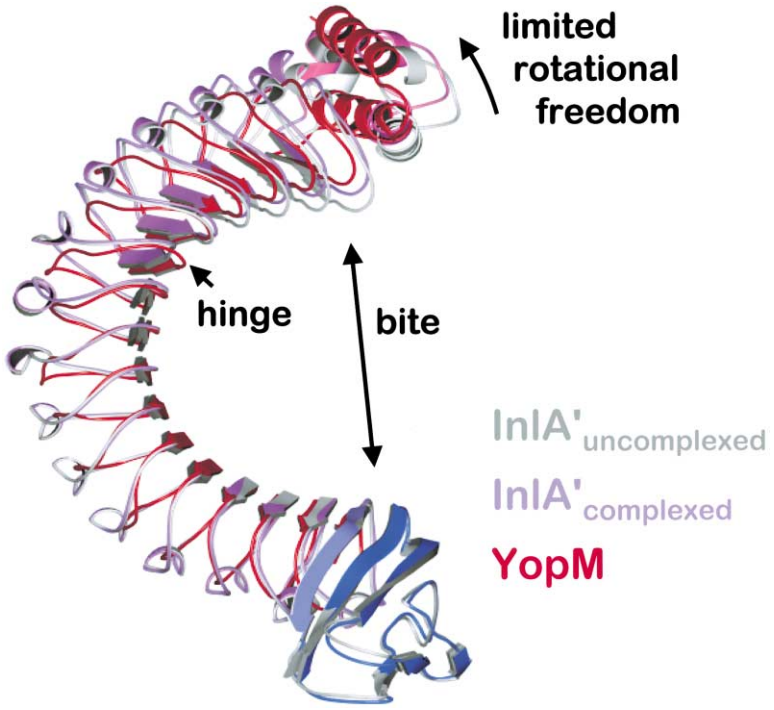

Figure 6. Induced Structural Flexibility in In1A

A superposition of the ten C-terminal repeats of uncomplexed InlA′ (light gray, unfilled binding site), hEC1–complexed InlA′ (pink/violet/blue) and YopM from *Yersinia pestis* (red, Evdokimov et al., 2001). In the uncomplexed state, the bite angle of InlA′ is smallest. On binding hEC1, the N-terminal part of InlA′ opens up, pivoting around LRR6. The deletion of one residue thus imparts a limited flexibility to an otherwise rigid LRR-domain. YopM represents the extended conformation lacking this deletion.

residue in InlA′ shortens the β strand of the repeat rather than the 3_{10}-helix or the intermediate loops. This disrupts the β sheet of InlA′ locally introducing its hinge. Lacking a hinge, YopM adopts a standard LRR-conformation over its entire length.

LRR-Domains as Protein-Protein Interaction Modules

Following the crystal structure of the ribonuclease inhibitor, LRR-proteins have been recognized as particularly versatile protein-protein interaction modules with a simple, building-block design and adaptable surface characteristics (Kobe and Kajava, 2001). LRR-domains occur most often in eukaryotes (Buchanan and Gay, 1996) but also in pathogenic bacteria, e.g., the internalin family of *Listeria monocytogenes* (Glaser et al., 2001), YopM of *Yersinia pestis* (Evdokimov et al., 2001), and IpaH of *Shigella flexneri* (Hartman et al., 1990).

Of all known LRR protein structures (other than internalins), YopM is structurally most similar to InlA′ (Figure 6). The only other complex of a long LRR-protein surrounding and binding a smaller target is that of the porcine ribonuclease inhibitor (RI)/ribonuclease A (RNase A) complex (Kobe and Deisenhofer, 1995). The overall similarity is striking though in detail there is very little correspondence between the two systems. The accessible surface area of binding is slightly larger in RI/RNase A (1250/1330Å^2) than in InlA'/hEC1 (1160/1240Å^2). In addition to the LRR-cavity, binding of RNase A by RI involves the surface adjacent to the cavity as well. InlA′, by contrast, exclusively binds hEC1 with residues within the LRR β strands or immediately adjacent to it. The dramatic difference in binding constants of the two complexes of many orders of magnitude appears to be due to the better match of polar and non-polar residues in RI/RNase A (polar 54/52%, non-polar 46/48%) than in InlA′/hEC1 (polar 58/37%, non-polar 42/63%).

Functionally the difference in binding affinities seems reasonable: RI needs to bind RNase A tightly to inhibit RNA cleavage. The function of InlA, by contrast, is initially to recognize E-cadherin. Attachment and uptake could then be achieved through the cooperativity of multiple associations rather than relying on the strength of the individual complexes while still allowing for the potential dissociation of the complex to achieve the release of the bacterium (see below).

Intermolecular Interfaces of E-Cadherin

E-cadherins are localized at the basolateral membrane of epithelial cells where they establish tight binding between neighboring cells in adherens junctions (Uemura, 1998; Gumbiner, 2000). Ca^{2+} is essential to achieve an extended cadherin conformation (Nagar et al., 1996) a prerequisite for generating *trans*-interactions between molecules from neighboring cells (Shapiro et al., 1995; Pertz et al., 1999). Neighboring cadherin molecules located on the same cell are thought to form *cis*-interactions, possibly before *trans*-interactions can occur (Pertz et al., 1999). An intermolecular contact observed in crystal structures of various cadherin fragments was initially interpreted to represent the *cis*-interaction interface (Shapiro et al., 1995). It involves an exchange of the N-terminal β strand of EC1 between neighboring molecules. In the structure of the complete extracellular domain of C-cadherin, this interface was found to link diametrically diverging molecules, possibly representing molecules from neighboring cells (Boggon et al., 2002). The interface was thus reinterpreted to represent the *trans*-interface.

Approaching an exposed epithelial membrane, a listerial cell would face an array of extended E-cadherin molecules. Potential *trans*-interaction interfaces would face outwards to facilitate homotopic interactions with E-cadherin molecules from a neighboring cell providing InlA′ (and hence *Listeria monocytogenes*) with a multitude of suitable docking surfaces. In the complex, InlA′ primarily binds β strands a and b and the connecting loop ab of hEC1. This surface is thus presumably the most exposed part of E-cadherin possibly supporting the identification of this interface as the *trans*-interaction surface (Boggon et al., 2002).

Note, however, that there is evidence indicating that *trans*-interactions may involve more than one extracellular domain (Chappuis-Flament et al., 2002). The identification of a single *trans*-interface for cadherin-cadherin interaction may need to be reevaluated.

Signaling of Bacterial Attachment to the Host Cytoplasm

We have described the complex required for the initial recognition of epithelial cells by *Listeria monocytogenes*. In addition to recognition, internalin, however, also single handedly achieves attachment and induces uptake into the host cell as latex beads covered only with InlA are phagocytosed within minutes of coming into contact with epithelial cells (Lecuit et al., 1997). Invasiveness of *Listeria monocytogenes* correlates with the amount of InlA presented at its surface (Dramsi et al., 1993). Similarly E-cadherin is presented in high local copy numbers on basolateral membranes of epithelial cells (Uemura, 1998). Irrespective of how *L. monocytogenes* binds to an exposed basolateral membrane (either by disrupting cell-cell interactions through its own virulence factors or by opportunistically binding to membranes exposed due to injury; Daniels et al., 2000), formation of a single InlA/E-cadherin complex (Figure 7) would imply the presence of additional InlA and E-cadherin molecules in the immediate vicinity. The consecutive complex formation by neighboring molecules (Figure 7, inset) would result in a local accumulation of complexes achieving macroscopic adhesion despite the relative weakness of the individual complex.

How is the signal of bacterial attachment transferred into the cytoplasm of the host cells and how is phagocytosis induced? Cadherins interact with the actin cytoskeleton through α- and β-catenins bound to their C-terminal, cytoplasmic domain (Kemler, 1993; Huber and Weis, 2001). Indeed, invasion of *L. monocytogenes* is dependent on an intact actin cytoskeleton (Lecuit et al., 2000). Cadherin-mediated adhesion is tightly regulated to allow for dynamic response to external or internal stimuli (Gumbiner, 2000). As cadherins play a part in processes like junction inhibition and need to respond to growth factors such as EGF and HGF, stimuli must be conveyed through the cadherin/catenin system both in an inside out and an outside in mechanism. These are as yet not fully understood but appear to be usurped by *Listeria monocytogenes* to induce a local re-

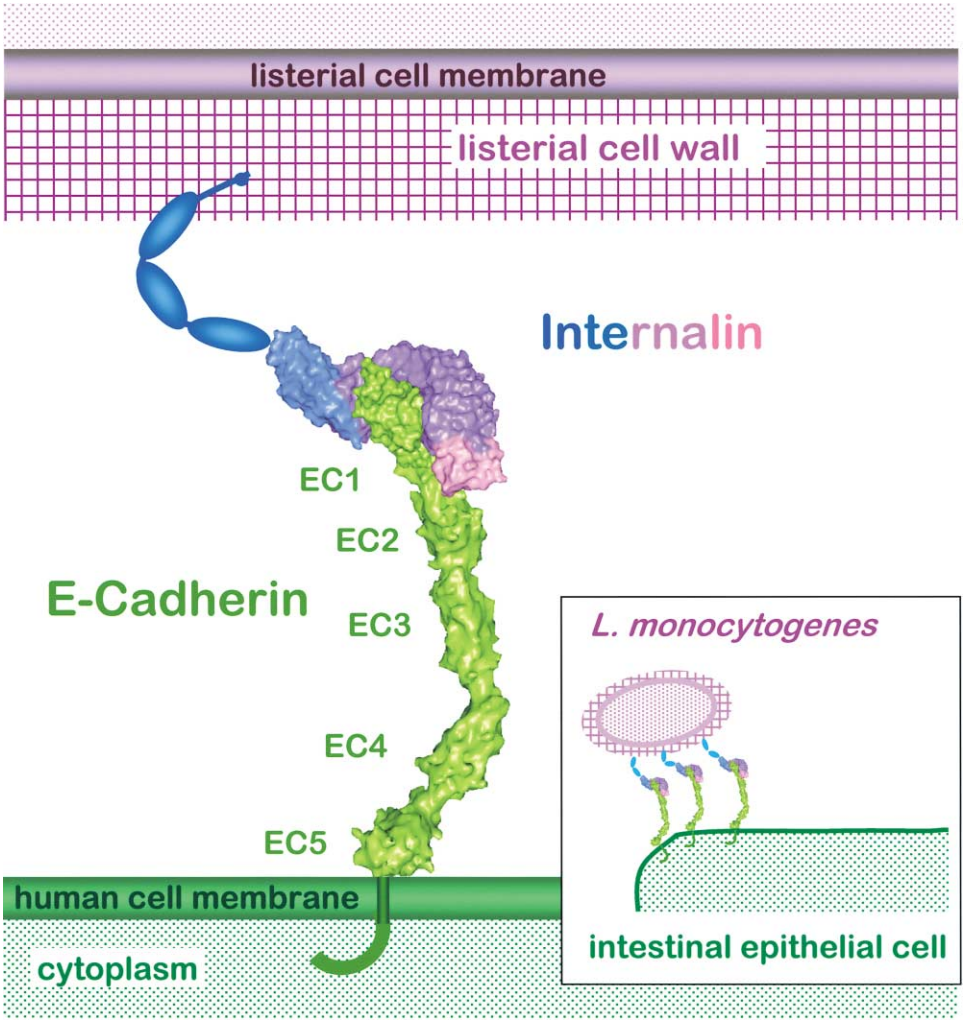

Figure 7. The Recognition Complex of Internalin and E-Cadherin in its Cellular Context

InlA, covalently bound to the cell wall of *L. monocytogenes* recognizes and binds E-cadherin. Known protein structures are represented by molecular surfaces: hEC2-hEC5 are modeled on C-cadherin (Boggon et al., 2002). C-terminal regions of both molecules are depicted schematically only. Inset: Both internalin and E-cadherin are present in high copy numbers on the surface of their respective cells.

arrangement of the cytoskeleton (Cossart and Lecuit, 1998).

InlA-induced conformational changes in hEC1 are confined to the N-terminal β strand a (Figure 3). These changes do not, however, influence the Ca^{2+} binding sites between EC1 and EC2 (see above). It is therefore difficult to envisage a conformational signal that could be communicated through the extracellular and the transmembrane domains of E-cadherin to the cytoplasm. As InlA uniformly covers the bacterial surface (Lebrun et al., 1996) the attachment process described, initially covering only a small area of the host cell, could spread enlarging the attachment surface. As previously postulated for the interaction of invasin from *Yersinia* spp. with integrins (Isberg, 1991), this could lead to a zipper-like activity promoting adhesion and finally uptake of the bacterium. Additional forces required for induced bacterial uptake would result from tensile forces due to the tethering interactions of E-cadherins to the actin cytoskeleton through adaptor molecules such as the catenins and vinculin.

Interestingly, complex formation is Ca^{2+}-dependent (see above). The Ca^{2+}-concentration in the intestinal compartment is ~2 mM, presumably sufficient to allow recognition and binding of InlA (*L. monocytogenes*) to E-cadherin (epithelial cell) followed by induction of bacterial phagocytosis. Engulfed within the phagosome, the bacterium secretes listeriolysin O, a cytolysin (Glomski et al., 2002), which punctures the vacuolar membrane reducing the Ca^{2+}-concentration to cytosolic levels (~2 nM). Reduced Ca^{2+}-concentrations would reduce the affinity of InlA for E-cadherin possibly helping to release the bacterium from the vacuolar membrane and allowing it to escape into the cytosol.

Conclusions

The 3-dimensional structure of the InlA′/hEC1 complex presented provides an unprecedented view of the first critical events of *Listeria* infection: the adhesion to the host cell epithelium (Figure 7) triggers the subsequent invasion of individual host cells, which normally are non-

Table 1. Data Collection and Refinement Statistics

Data collection[a]			
Data set	**InlA′ C2-I**	**InlA′ C2-II**	**InlA′/hEC1 complex**
Space group	C2	C2	$P2_12_12_1$
Unit cell lengths (Å)	95.9, 55.9, 97.8	85.8, 68.0, 153.6	55.4, 86.8, 110.7
Monoclinic angle (°)	113.1	103.3	-
Molecules/asym.unit	1	2	1 + 1
Resolution range (Å)	20-1.6 (1.63–1.60)	20–1.5 (1.53–1.50)	25–1.8 (1.86–1.80)
R_{merge} (%)	4.8 (31.7)	5.1 (14.4)	6.2 (38.5)
I/σ_I	23.9 (3.7)	22.1 (9.7)	14.4 (3.4)
Completeness (%)	99.5 (99.2)	89.9 (90.7)	92.0 (84.3)
Redundancy	3.6 (3.5)	3.1 (2.7)	6.2 (4.5)
Unique reflections	62,613	122,892	46,306
Refinement			
Resolution	20–1.6	158–1.5	69–1.8
R (%)	14.1	15.9	16.6
R_{free} (%)	17.3	19.3	22.2
Number of reflections: working/test	59,440/3,170	116,651/6,192	41,618/2,344
Water molecules	719	1,420	541
$Ca^{2+}/Cl^{-}/SO_4^{2-}$	1/0/7	0/0/0	2/3/0
Side chains in multiple conformations	15	17+19	23+7
Overall B factor (Å^2)	18.2	14.0	23.6
Rmsd bond lengths (Å)	0.018	0.010	0.018
Rmsd bond angles (°)	1.75	1.42	1.78
Ramachandran Plot: allowed/additional/disallowed (%)	77.6/24.4/0	75.5/24.5/0	78.5/21.5/0.2

[a] Numbers in parentheses indicate values corresponding to the highest resolution shell.

phagocytic. It is evident that this interaction is not accidental, but rather a perfect adaptation as a result of prolonged evolutionary crosstalk between pathogen and host cells. The structure of the complex reveals an intricate network of interactions sufficient for recognition, adhesion, and invasion. Binding studies including mutational analyses, however, indicate that these interactions are weak enough to dissociate the bacterium from E-cadherin following uptake into the phagosome and finally into the host cytosol. The understanding of the fine molecular details of the host-pathogen interaction not only provides the basis for the possible development of novel therapeutic approaches but also detailed insights in the functions of prominent eukaryotic receptors like E-cadherin.

Experimental Procedures

Cloning, Protein Purification, and Mutagenesis

Bacterial DNA coding for residues 36 to 496 of InlA from *Listeria monocytogenes* was cloned by PCR into the pGEX-6P1 vector (Amersham) and expressed as a cytoplasmic glutathione-S-transferase (GST) fusion protein. Purification steps included affinity chromatography, Precision Protease cleavage of the N-terminal GST-tag, and MonoQ anion exchange chromatography (Amersham). The protein, which retains five additional N-terminal amino acids of the protease cleavage site, was concentrated to ~10 mg/ml.

DNA encoding the first 100 amino acids of hEC1 was cloned by PCR from a human cDNA library into the pGEX-6P1 vector. The protein was subsequently prepared using a similar production and purification strategy as outlined for InlA.

Site-directed mutations of residues involved in the InlA′/hEC1 interface were introduced into both proteins using the QuikChange Mutagenesis method (Stratagene).

Crystallization

Both InlA′ and InlA′/ hEC1 were crystallized at 20°C using hanging drop vapor diffusion setups. InlA′ crystallized in two unrelated, monoclinic crystal forms (space group C2) hereafter referred to as C2-I and C2-II. Both were obtained using a protein concentration of ~10 mg/ml mixed 1:1 with reservoir solutions containing 10% (w/v) PEG 4000, 100 mM MES/Tris [pH 6.0], and 100 mM ammonium sulfate.

For the InlA′/hEC1 complex, stoichiometric amounts of both proteins were preincubated for 1 hr at 20°C before crystallization; total protein concentration was ~10 mg/ml. Crystals of the InlA′/hEC1 complex were obtained using 26% PEG 4000, 0.1 M MES/Tris [pH 7.0], and 100 mM sodium acetate. The crystal used in this study grew in the presence of 50 mM $CaCl_2$ in the reservoir solution. For cryoprotection, 40% PEG 400 (v/v) was added to the reservoir solution for InlA′ and 10% PEG 400 (v/v) for InlA′/hEC1.

Structure Determination

X-ray data were collected using synchrotron radiation (λ = 1.05 Å) and a MAR CCD detector at beamline BW6 (DESY Hamburg, Germany). X-ray data were processed using DENZO/SCALEPACK (Otwinowski and Minor, 1997) and TRUNCATE (CCP4, 1994). Molecular replacements were performed using AMORE (Navaza, 1994). Initial refinement and manual rebuilding were performed using CNS (Brünger et al., 1998) and O (Jones et al., 1991). Final refinement and solvent incorporation was performed using a combination of REFMAC5 (Murshudov et al., 1997) and ARP_WARP (Lamzin and Wilson, 1993) excluding 5% of the data for free R-factor calculation (Brünger, 1992).

The structure of InlA′ was solved by molecular replacement using a model built from InlH′ (Schubert et al., 2001). The structure was refined at 1.6 Å resolution. The C-terminal residue 496 is not visible in any of the electron density maps. Disordered regions vary (Table 1). Molecular replacement of crystal form C2-II using the refined structure of InlA′ from C2-I located two molecules per asymmetric unit related by a translation of half a unit cell along the c-axis plus a small shift out of the ac-plane. Each InlA′ is located near a crystal-

lographic 2-fold axis, yielding intertwined LRR-domains. The structure was refined at 1.5 Å resolution (Table 1). Molecule A (C2-II_A) and B (C2-II_B) are structurally practically identical. The mean r.m.s. deviation is 0.30 Å for all backbone atoms.

For the complex of InlA′ and hEC1, molecular replacement using InlA′ (crystal form C2-II) as a search model resulted in a suitable solution in a first low-resolution (3 Å) data set. After initial refinement of InlA′, murine EC1 could manually be placed into the as yet discontinuous electron density of the inner void of the curved InlA′. The final model at 1.8 Å resolution contains residues 36 to 495 of InlA (residues 464–7 disordered) and residues −3 to 100 of hEC1 (Table 1).

The structures were validated using PROCHECK (Laskowski et al., 1993) and CHECKIT (CCP4, 1994).

Structure Comparisons, Modeling, and Interface Analysis

Crystal structure superpositions were performed using LSQKAB (CCP4, 1994). Hydrogen bonds and salt bridges between InlA′ and hEC1 (≤ 3.6 Å) and hydrophobic and unfavorable polar/non-polar interactions (≤ 4.0 Å) were determined using CONTACT (CCP4, 1994). Accessible surface areas (ASA) of interactions were determined using the Protein-Protein-Interaction-Server (www.biochem.ucl.ac.uk/bsm/PP/server/).

Molecular depictions were prepared using MOLSCRIPT (Kraulis, 1991), surfaces by GRASP (Nicholls et al., 1993), and electron density manipulation using CONSCRIPT (Lawrence and Bourke, 2000).

Binding Studies and Analytical Ultracentrifugation Experiments

Affinity chromatography was used to analyze InlA′/hEC1 complex formation. InlA′ and hEC1 were incubated over night with (1) glutathione-sepharose (GS), (2) GS-bound glutathione-S-transferase (GST) as controls and with either (1) GS-bound GST–hEC1 fusion protein or (2) GS-bound GST–InlA′ fusion proteins and eluted. The effect of Ca^{2+} (0 to 150 mM) and pH (4 to 9) was systematically tested. Bound protein was analyzed by Coomassie-stained SDS-PAGE.

A more detailed binding study was performed by analytical ultracentrifugation. Detecting the interaction of two macromolecules is based on the observed increase in mass of the complex as compared to its components. Its sedimentation coefficient is thus larger which may be detected in a strong gravitational field. Sedimentation was performed in a Beckman XL-A analytical ultracentrifuge equipped with UV absorption optics and an 8-place analytical rotor. Experiments were performed in 5 mM HEPES, [pH 7.0] with the addition of 20 mM $CaCl_2$ based on the results of the binding studies described above.

Sedimentation profiles were recorded at 20°C and 45,000 rpm with a total protein absorption of 0.6 at 280 nm corresponding to 10–30 μM hEC1 and 10–20 μM InlA′. Sedimentation rate constants and relative boundary heights were evaluated by fitting a sum of Gaussians as described (Machner et al., 2001). The sedimentation coefficients of uncomplexed hEC1 and InlA′ are 1.5 and 3.2 S. These are insensitive to the addition of 20 mM $CaCl_2$. Boundaries with sedimentation coefficients larger than 3.3 S were interpreted to indicate interactions between the two proteins. S-values were corrected for buffer viscosity and density and are reported as S(20°,water)-values. No concentration correction was applied. Concentrations of free and bound proteins were derived from the relative height of the sedimenting boundaries. A binding constant was estimated based on these concentrations.

Acknowledgments

We thank Torsten Hain (University of Giessen, Germany) for the expression clone of InlA′; Matthias Krause and Daniel Kloer for assistance in cloning human E-cadherin; and the staff of beamline BW6 at DESY Hamburg for their support during synchrotron data collection. This work was funded by the BMBF, Bonn, Germany (to D.W.H.) and in part by the Deutsche Forschungsgemeinschaft through SFB 535 (TP A5 to E.D.).

Received: August 7, 2002
Revised: October 15, 2002

References

Bierne, H., Mazmanian, S.K., Trost, M., Pucciarelli, M.G., Liu, G., Dehoux, P., Jänsch, L., Garcia-del Portillo, F., Schneewind, O., and Cossart, P. (2002). Inactivation of the srtA gene in *Listeria monocytogenes* inhibits anchoring of surface proteins and affects virulence. Mol. Microbiol. *43*, 869–881.

Boggon, T.J., Murray, J., Chappuis-Flament, S., Wong, E., Gumbiner, B.M., and Shapiro, L. (2002). C-Cadherin ectodomain structure and implications for cell adhesion mechanism. Science *296*, 1308–1313.

Brünger, A.T. (1992). Free R-value: a novel statistical quantity for assessing the accuracy of crystal structures. Nature *355*, 472–475.

Brünger, A.T., Adams, P.D., Clore, G.M., DeLano, W.L., Gros, P., Grosse-Kunstleve, R.W., Jiang, J.S., Kuszewski, J., Nilges, M., Pannu, N.S., et al. (1998). Crystallography & NMR system: a new software suite for macromolecular structure determination. Acta Crystallogr. *D54*, 905–921.

Buchanan, S.G., and Gay, N.J. (1996). Structural and functional diversity in the leucine rich repeat family of proteins. Prog. Biophys. Mol. Biol. *65*, 1–44.

Cabanes, D., Dehoux, P., Dussurget, O., Frangeul, L., and Cossart, P. (2002). Surface proteins and pathogenic potential of *Listeria monocytogenes*. Trends Microbiol. *10*, 238–245.

Chappuis-Flament, S., Wong, E., Hicks, L.D., Kay, C.M., and Gumbiner, B.M. (2002). Multiple cadherin extracellular repeats mediate homophilic binding adhesion. J. Cell Biol. *154*, 231–243.

CCP4 (Collaborative Computational Project 4) (1994). The CCP4 suite: programs for protein crystallography. Acta Crystallogr. D *50*, 760–763.

Cossart, P., and Lecuit, M. (1998). Interactions of *Listeria monocytogenes* with mammalian cells during entry and actin-based movement: bacterial factors, cellular ligands and signaling. EMBO J. *17*, 3797–3806.

Daniels, J.J.D., Autenrieth, I.B., and Goebel, W. (2000). Interaction of *Listeria monocytogenes* with the intestinal epithelium. FEMS Microbiol. Lett. *190*, 323–328.

Dramsi, S., Kocks, C., Foestier, C., and Cossart, P. (1993). Internalin-mediated invasion of epithelial cells by *Listeria monocytogenes* is regulated by the bacterial growth state, temperature and the pleiotropic activator *prfA*. Mol. Microbiol. *9*, 931–941.

Dramsi, S., Biswas, I., Maguin, E., Braun, L., Mastroeni, P., and Cossart, P. (1995). Entry of *Listeria monocytogenes* into hepatocytes requires expression of inlB, a surface protein of the internalin multigene family. Mol. Microbiol. *16*, 251–261.

Evdokimov, A.G., Anderson, D.E., Routzahn, K.M., and Waugh, D.S. (2001). Unusual molecular architecture of the *Yersinia pesitis* cytotoxin YopM: a leucine-rich repeat protein with the shortest repeating unit. J. Mol. Biol. *312*, 807–821.

Gaillard, J.L., Berche, P., Frehel, C., Gouin, E., and Cossart, P. (1991). Entry of *L. monocytogenes* into cells is mediated by internalin, a repeat protein reminiscent of surface antigens from gram-positive cocci. Cell *65*, 1127–1141.

Galan, J.E. (2000). Alternative strategies for becoming an insider: lessons from the bacterial world. Cell *103*, 363–366.

Garandeau, C., Réglier-Poupet, H., Dubail, I., Berezzi, J.-L., Berche, P., and Charbit, A. (2002). The sortase SrtA of *Listeria monocytogenes* is involved in processing of internalin and in virulence. Infect. Immun. *70*, 1382–1390.

Glaser, P., Frangeul, L., Buchrieser, C., Rusniok, C., Amend, A., Baquero, F., Berche, P., Bloecker, H., Brandt, P., Chakraborty, T., et al. (2001). Comparative genomics of *Listeria* species. Science *294*, 849–852.

Glomski, I.J., Gedde, M.M., Tsang, A.W., Swanson, J.A., and Portnoy, D.A. (2002). The *Listeria monocytogenes* hemolysin has an acidic pH optimum to compartmentalize activity and prevent damage to infected host cells. J. Cell Biol. *156*, 1029–1038.

Gumbiner, B.M. (2000). Regulation of cadherin adhesive activity. J. Cell Biol. *148*, 399–403.

Hartman, A.B., Venkatesan, M., Oaks, E.V., and Buysse, J.M. (1990).

Sequence and molecular characterization of a multicopy invasion plasmid antigen gene, *ipaH*, of *Shigella flexneri*. J. Bacteriol. *172*, 1905–1915.

Huber, A.H., and Weis, W.I. (2001). The structure of the β-catenin/E-cadherin complex and the molecular basis of diverse ligand recognition by β-catenin. Cell *105*, 391–401.

Isberg, R.R. (1991). Discrimination between intracellular uptake and surface adhesion of bacteria. Science *252*, 934–938.

Jones, T.A., Zou, J.Y., Cowan, S.W., and Kjeldgaard, M. (1991). Improved methods for building protein models in electron density maps and the location of errors in these models. Acta Crystallogr. *A47*, 110–119.

Kahn, R.A., Fu, H., and Roy, C.R. (2002). Cellular hijacking: a common strategy for microbial infection. Trends Biochem. Sci. *27*, 308–314.

Kemler, R. (1993). From cadherins to catenins: cytoplasmic protein interactions and regulation of cell adhesion. Trends Genet. *9*, 317–321.

Kobe, B., and Deisenhofer, J. (1995). A structural basis of the interactions between leucine-rich repeats and protein ligands. Nature *374*, 183–186.

Kobe, B., and Kajava, A.V. (2001). The leucine-rich repeat as a protein recognition motif. Curr. Opin. Struct. Biol. *11*, 725–732.

Kraulis, P.J. (1991). MOLSCRIPT: a program to produce both detailed and schematic plots or protein structures. J. Appl. Crystallogr. *24*, 946–950.

Lamzin, V.S., and Wilson, K.S. (1993). Automated refinement of protein models. Acta Crystallogr. *D49*, 129–147.

Laskowski, R.A., MacArthur, M.W., Moss, D.S., and Thornton, J.M. (1993). PROCHECK: a program to check the stereochemical quality of protein structures. J. Appl. Crystallogr. *26*, 283–291.

Lawrence, M.C., and Bourke, P. (2000). CONSCRIPT: a program for generating electron density isosurfaces for presentation in protein crystallography. J. Appl. Crystallogr. *33*, 990–991.

Leahy, D.J. (1997). Implications of atomic-resolution structures for cell adhesion. Annu. Rev. Cell Dev. Biol. *13*, 363–393.

Lebrun, M., Mengaud, J., Ohayon, H., Nato, F., and Cossart, P. (1996). Internalin must be present on the bacterial surface to mediate entry of *Listeria monocytogenes* into epithelial cells. Mol. Microbiol. *21*, 579–592.

Lecuit, M., Ohayon, H., Braun, L., Mengaud, J., and Cossart, P. (1997). Internalin of *Listeria monocytogenes* with an intact leucine-rich repeat region is sufficient to promote internalization. Infect. Immun. *65*, 5309–5319.

Lecuit, M., Dramsi, S., Gottardi, C., Fedor-Chaiken, M., Gumbiner, B., and Cossart, P. (1999). A single amino acid in E-cadherin responsible for host specificity towards the human pathogen *Listeria monocytogenes*. EMBO J. *18*, 3956–3963.

Lecuit, M., Hurme, R., Pizarro-Cerda, J., Ohayon, H., Geiger, B., and Cossart, P. (2000). A role for α- and β-catenins in bacterial uptake. Proc. Natl. Acad. Sci. USA *97*, 10008–10013.

Lecuit, M., Vandormael-Pournin, S., Lefort, J., Huerre, M., Gounon, P., Dupuy, C., Babinet, C., and Cossart, P. (2001). A transgenic model for listeriosis: role of internalin in crossing the intestinal barrier. Science *292*, 1722–1725.

Lingnau, A., Domann, E., Hudel, M., Bock, M., Nichterlein, T., Wehland, J., and Chakraborty, T. (1995). Expression of the *Listeria monocytogenes* EGD *inlA* and *inlB* genes, whose products mediate bacterial entry into tissue culture cell lines, by PrfA-dependent and -independent mechanisms. Infect. Immun. *63*, 3896–3903.

Lo Conte, L., Chothia, C., and Janin, J. (1999). The atomic structure of protein-protein recognition sites. J. Mol. Biol. *285*, 2177–2198.

Lorber, B. (1997). Listeriosis. Clin. Infect. Dis. *24*, 1–9.

Machner, M.P., Urbanke, C., Barzik, M., Otten, S., Sechi, A.S., Wehland, J., and Heinz, D.W. (2001). ActA from the human pathogen *Listeria monocytogenes* is a monomer simultaneously interacting with four Ena/VASP homology 1 domains. J. Biol. Chem. *276*, 40096–40103.

Marino, M., Braun, L., Cossart, P., and Ghosh, P. (1999). Structure of the InlB leucine-rich repeats, a domain that triggers host cell invasion by the bacterial pathogen *L. monocytogenes*. Mol. Cell *4*, 1063–1072.

Mengaud, J., Ohayon, H., Gounon, P., Mege, R.M., and Cossart, P. (1996). E-cadherin is the receptor for internalin, a surface protein required for entry of *L. monocytogenes* into epithelial cells. Cell *84*, 923–932.

Murshudov, G.N., Vagin, A.A., and Dodson, E.H. (1997). Refinement of macromolecular structures by the maximum-likelihood method. Acta Crystallogr. *D53*, 240–255.

Nagar, B., Overduin, M., Ikura, M., and Rini, J.M. (1996). Structural basis of calcium-induced E-cadherin rigidification and dimerization. Nature *380*, 360–364.

Navaza, J. (1994). AMoRe: an automated package for molecular replacement. Acta Crystallogr. *A50*, 157–163.

Nicholls, A., Bharadwaj, R., and Honig, B. (1993). GRASP: a graphical representation and analysis of surface properties. Biophys. J. *64*, A166.

Otwinowski, Z., and Minor, W. (1997). Processing of X-ray diffraction data collected in oscillation mode. Meth. Enzymol. *276*, 307–326.

Overduin, M., Harvey, T.S., Bagby, S., Tong, K.I., Yau, P., Takeichi, M., and Ikura, M. (1995). Solution structure of the epithelial cadherin domain responsible for selective cell adhesion. Science *267*, 386–389.

Pertz, O., Bozic, D., Koch, A.W., Fauser, C., Brancaccio, A., and Engel, J. (1999). A new crystal structure, Ca^{2+} dependence and mutational analysis reveal molecular details of E-cadherin homoassociation. EMBO J. *18*, 1738–1747.

Pieters, J. (2001). Evasion of host cell defense mechanisms by pathogenic bacteria. Curr. Opin. Immunol. *13*, 37–44.

Schlech, W.F. (2000). Foodborne listeriosis. Clin. Infect. Dis. *31*, 770–775.

Schubert, W.-D., Gobel, G., Diepholz, M., Darji, A., Kloer, D., Hain, T., Chakraborty, T., Wehland, J., Domann, E., and Heinz, D.W. (2001). Internalins from the human pathogen *Listeria monocytogenes* combine three distinct folds into a contiguous internalin domain. J. Mol. Biol. *312*, 783–794.

Shapiro, L., Fannon, A.M., Kwong, P.D., Thompson, A., Lehmann, M.S., Grubel, G., Legrand, J.F., Als-Nielsen, J., Colman, D.R., and Hendrickson, W.A. (1995). Structural basis of cell-cell adhesion by cadherins. Nature *374*, 327–337.

Steinberg, M.S., and McNutt, P.M. (1999). Cadherins and their connections: adhesion junctions have broader functions. Curr. Opin. Cell Biol. *11*, 554–560.

Tamura, K., Shan, W.S., Hendrickson, W.A., Colman, D.R., and Shapiro, L. (1998). Structure-function analysis of cell adhesion by neural (N-)cadherin. Neuron *20*, 1153–1163.

Uemura, T. (1998). The cadherin superfamily at the synapse: more members, more missions. Cell *93*, 1095–1098.

Accession Numbers

The coordinates of the structures have been deposited with the Protein Data Bank (accession numbers 1o6s, 1o6t and 1o6v).